MFASIS fit and interpolation errors in RTTOV v13 as a function of observation geometry

Christina Stumpf[1], Leonhard Scheck[1,2], and Christina Köpken-Watts[1]

[1] *DWD*
[2] *Hans-Ertel-Zentrum/LMU München*

This note was compiled to help users judge the expected accuray of MFASIS forward simulations for the various instruments for which look-up-tables (LUTs) are currently provided as a function of the observation geometry (satellite and sun angles). It addresses the magnitude of errors of MFASIS with respect to DOM due to

- the least squares fitting of the Fourier coefficients in the generation of the LUTs and
- the interpolation in the LUTs for the evaluation of the reflectance function in the MFASIS simulation.

Additional errors (not covered here) result from the approximations made in the input of MFASIS, where a limited set of parameters is taken to represent an atmospheric profile, especially the cloud characteristics. For more details and evaluation of additional aspects and overall accuracy please refer to the RTTOV-13 Science and Valiation report [2]. Note that the results shown here are only for the Deff scheme, but broadly similar results are expected for the OPAC cloud liquid water properties. For details on MFASIS and its implementation in RTTOV refer to [1, 2].

The difference of the MFASIS reflectance (R_M) and DOM reflectance (R_D)

$$\Delta R = R_M(\theta, \theta_0, \alpha, A, \tau_w, \tau_i, r_w, r_i) - R_D(\theta, \theta_0, \alpha, A, \tau_w, \tau_i, r_w, r_i) \tag{1}$$

is computed for many idealised atmospheric scenes. These scenes correspond to a Rayleigh atmosphere containing a homogeneous liquid water cloud located between 2km and 4km and a homogeneous ice cloud located between 6km and 8km above a surface at sea level with albedo A. The total optical depths of the water and ice clouds are τ_w and τ_i, the water and ice effective particle sizes are set to r_w and r_i, respectively. The observation geometry is characterised by the satellite zenith angle θ, solar zenith angle θ_0 and the scattering angle α ($\alpha = 0°$ is defined as forward scattering here).

In the following figures, ΔR is considered as a function of the scattering angle α and the maximum of the solar and satellite zenith angle, and results in the $\alpha \times \max(\theta, \theta_0)$ plane are shown in figs. 1 to 26 for all instruments and channels for which MFASIS LUTs are currently available. Plots are included for ABI (GOES-16), AHI (Himawari-8), AMI (GEO-KOMPSAT-2A), SEVIRI (METEOSAT-11), EPIC (DSCOVR, on the NOAA Deep Space Climate Observatory) and FCI (MTG-I1), and errors for the same instruments on other platforms are nearly identical. Note that the near-infrared channel around 1.6μm is available from RTTOVv13.1 on only.

The figures illustrate the mean value of ΔR, the maximum and mean value of $|\Delta R|$, and the 99th percentile of $|\Delta R|$, where MFASIS and DOM reflectances of 100 idealised profiles with arbitrary A, τ_w, τ_i, r_w and r_i have been used in each bin ($5° \times 5°$ for ABI, AHI, AMI, SEVIRI and $1° \times 5°$ for EPIC). Average and maximum values of the ABI, AHI, AMI, SEVIRI and FCI results in the region defined by $50° < \alpha < 170°$ and $\max(\theta, \theta_0) < 80°$ (dashed lines in figs. 1 to 17 and 22 to 26) are also provided in the plots. For EPIC, the corresponding values have been extracted for the region defined by $164° < \alpha < 176°$ and $\max(\theta, \theta_0) < 80°$ (dashed lines in figs. 18 to 21).

Generally, the errors for all instruments are very small for most viewing conditions and larger inaccuracies due to fit and interpolation errors in MFASIS are found only for large zenith angles, small scattering angles

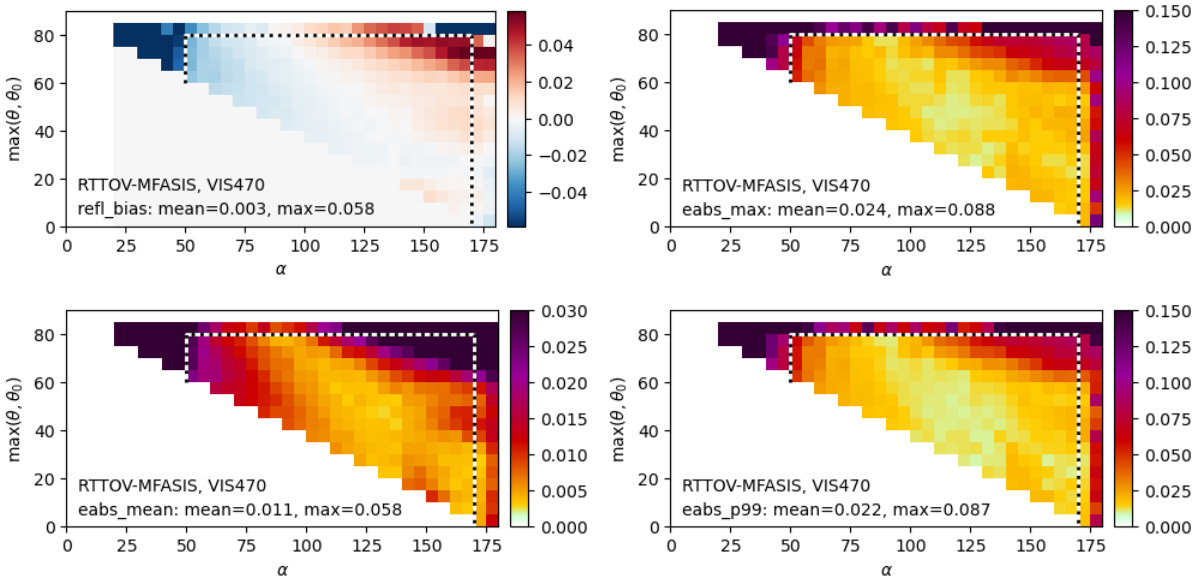

Figure 1: Mean reflectance fit and interpolation errors (upper left panel) and maximum (upper right panel), mean (lower left panel) and 99th percentile (lower right panel) of the absolute reflectance fit and interpolation errors for the 470nm ABI channel (GOES-16) as a function of α and $\max(\theta, \theta_0)$. For each bin MFASIS was compared to DOM for 100 idealised profiles based on randomly chosen optical parameters A, τ_w, τ_i, r_w and r_i within the range of the MFASIS LUT limits, the angles were chosen randomly within the bin.

and the glory region ($\alpha > 170°$). Note that the EPIC instrument covers only a very limited range of large scattering angles, reaching noticeably into the backscatter glory region. Furthermore, results for channels with shorter wavelengths are more affected by molecular Rayleigh scattering and exhibit larger errors.

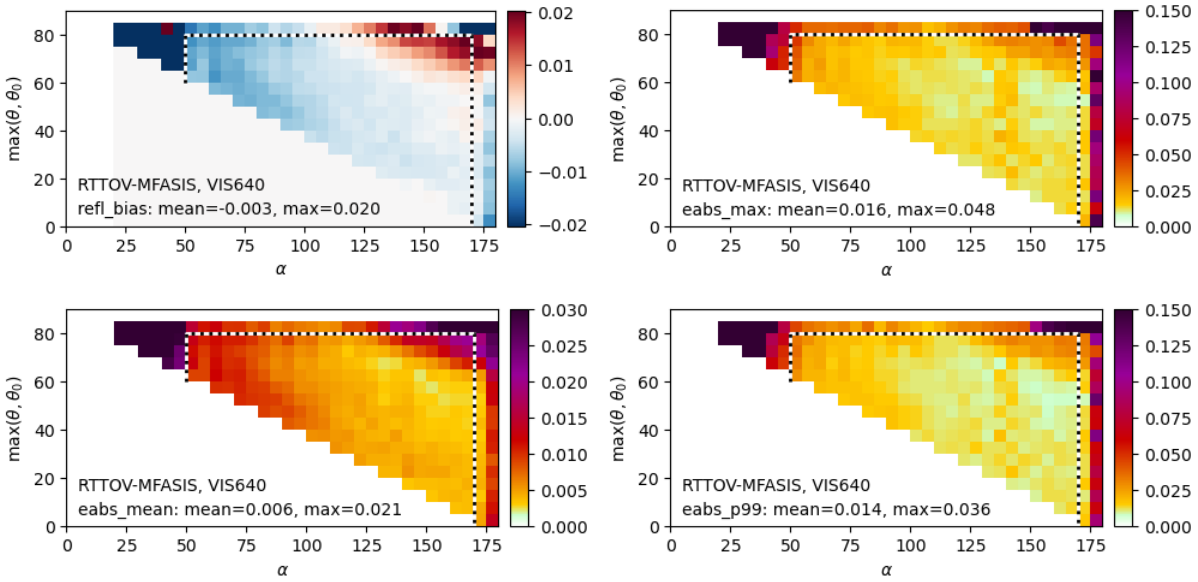

Figure 2: Same as fig. 1 but for the 640nm ABI channel (GOES-16).

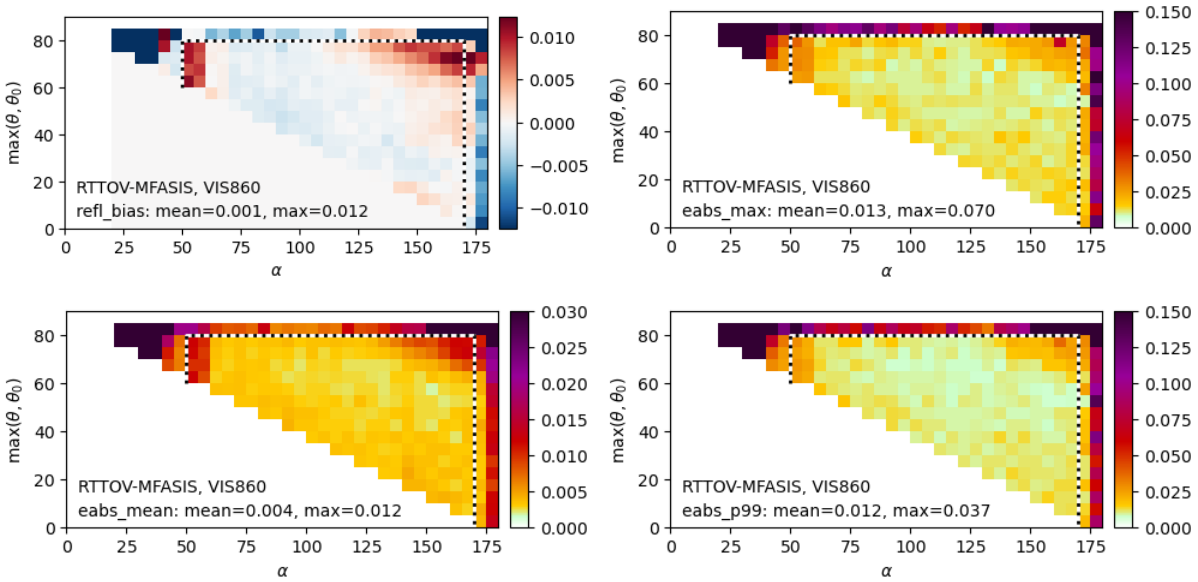

Figure 3: Same as fig. 1 but for the 860nm ABI channel (GOES-16).

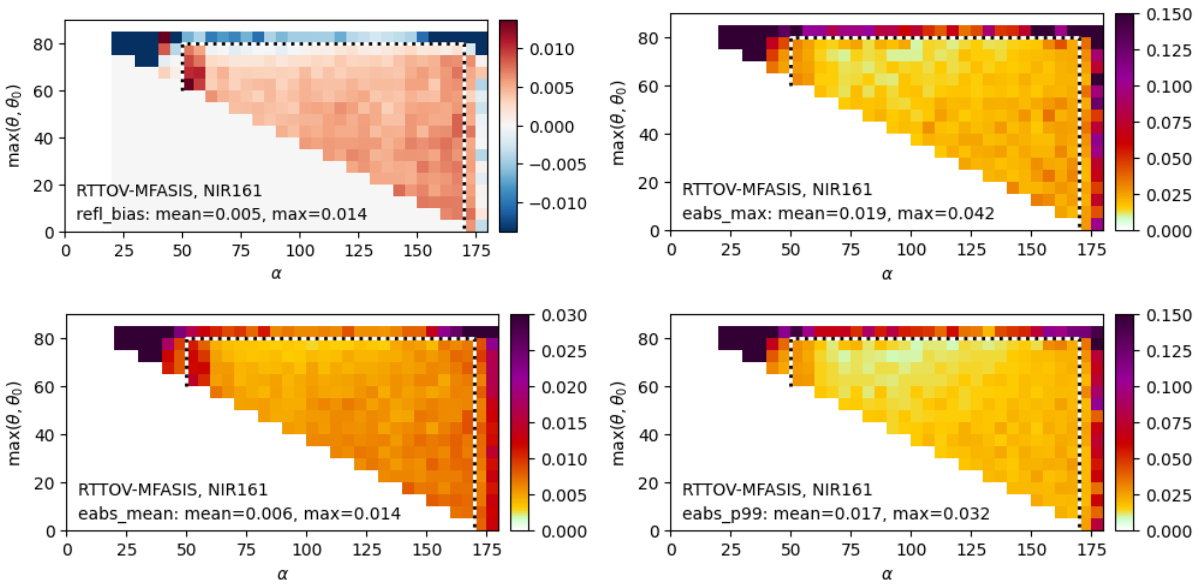

Figure 4: Same as fig. 1 but for the 1610nm ABI channel (GOES-16).

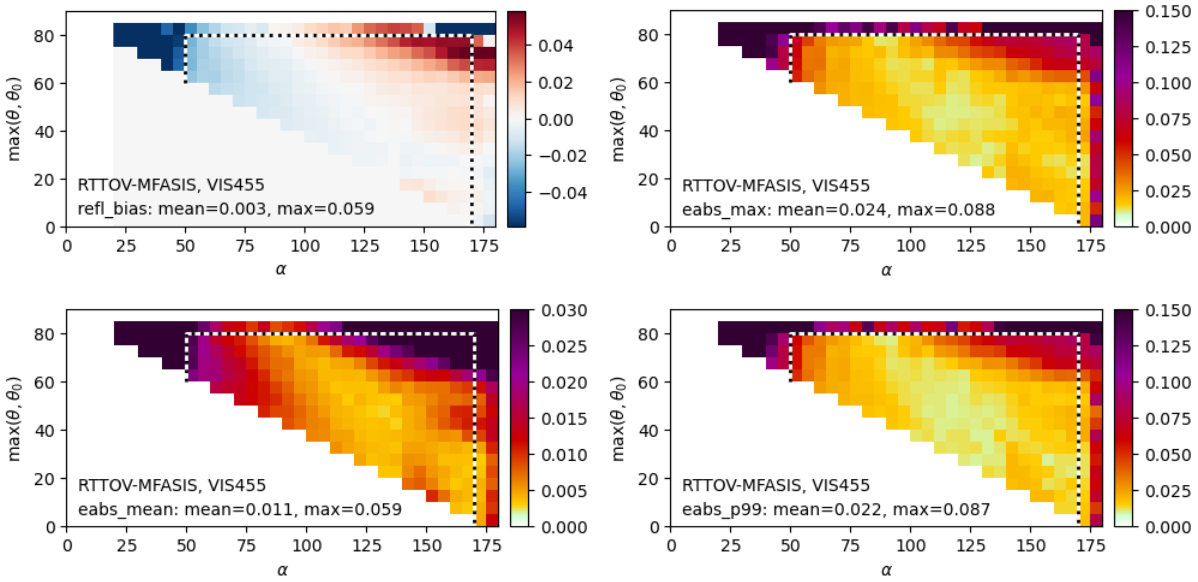

Figure 5: Same as fig. 1 but for the 455nm AHI channel (Himawari-8).

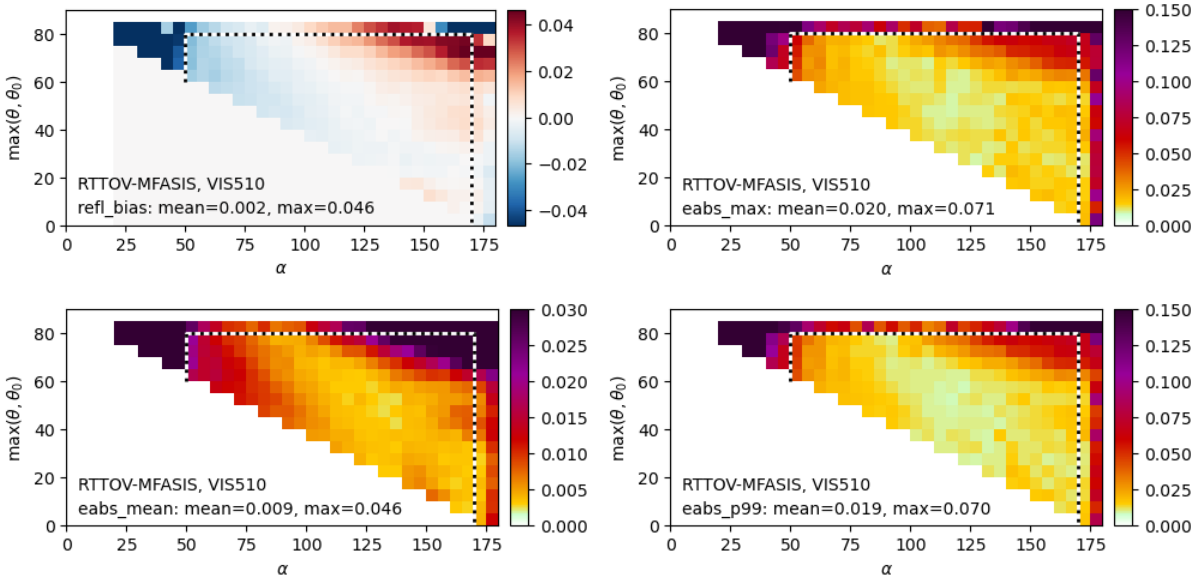

Figure 6: Same as fig. 1 but for the 510nm AHI channel (Himawari-8).

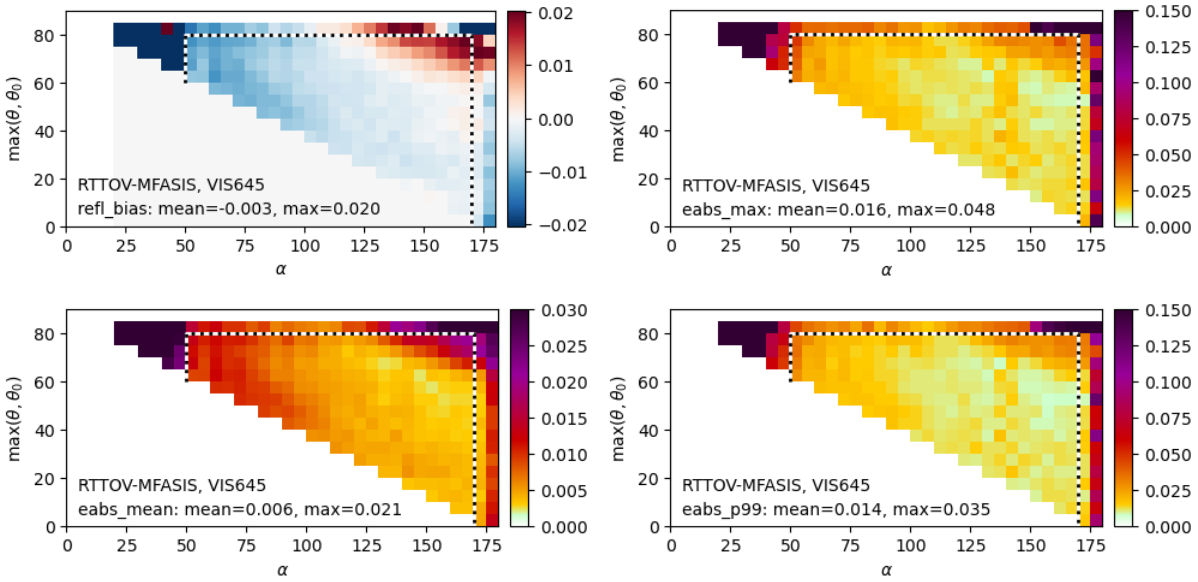

Figure 7: Same as fig. 1 but for the 645nm AHI channel (Himawari-8).

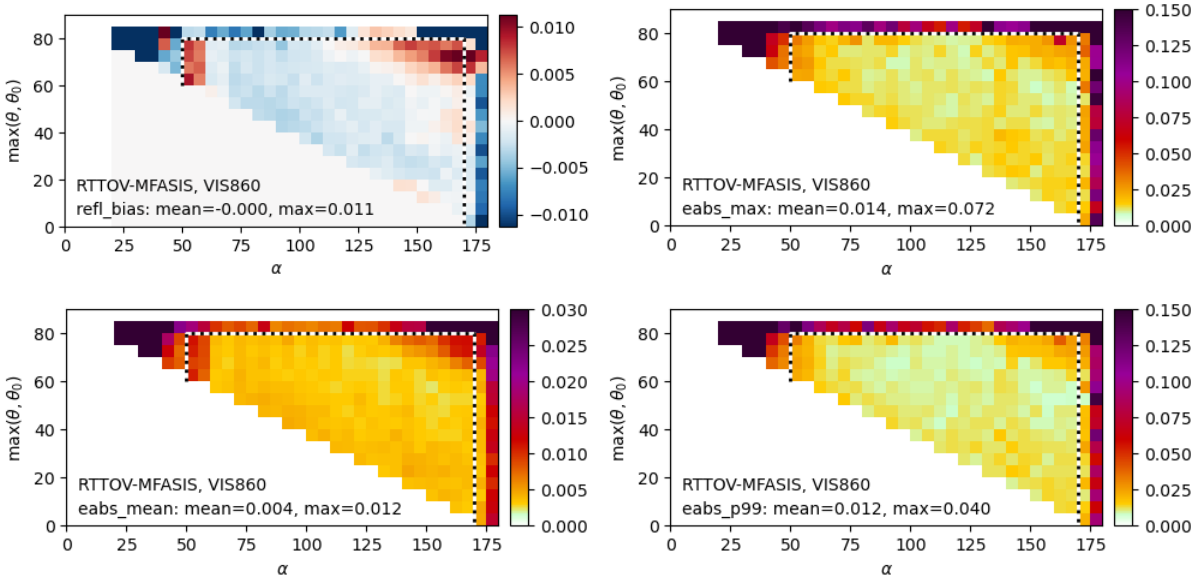

Figure 8: Same as fig. 1 but for the 860nm AHI channel (Himawari-8).

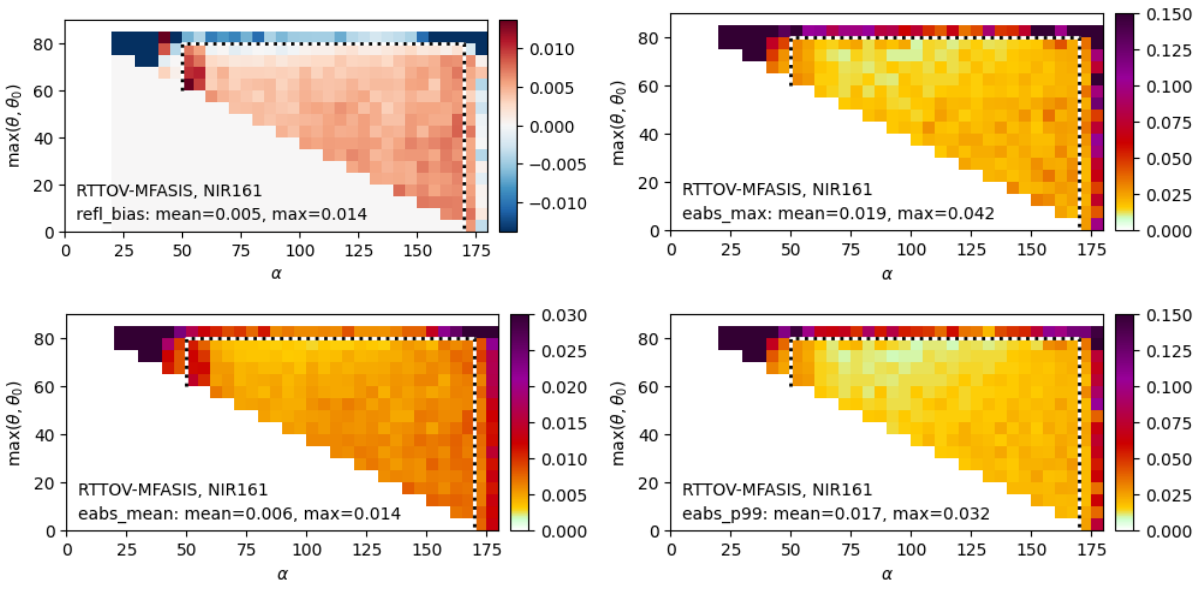

Figure 9: Same as fig. 1 but for the 1610nm AHI channel (Himawari-8).

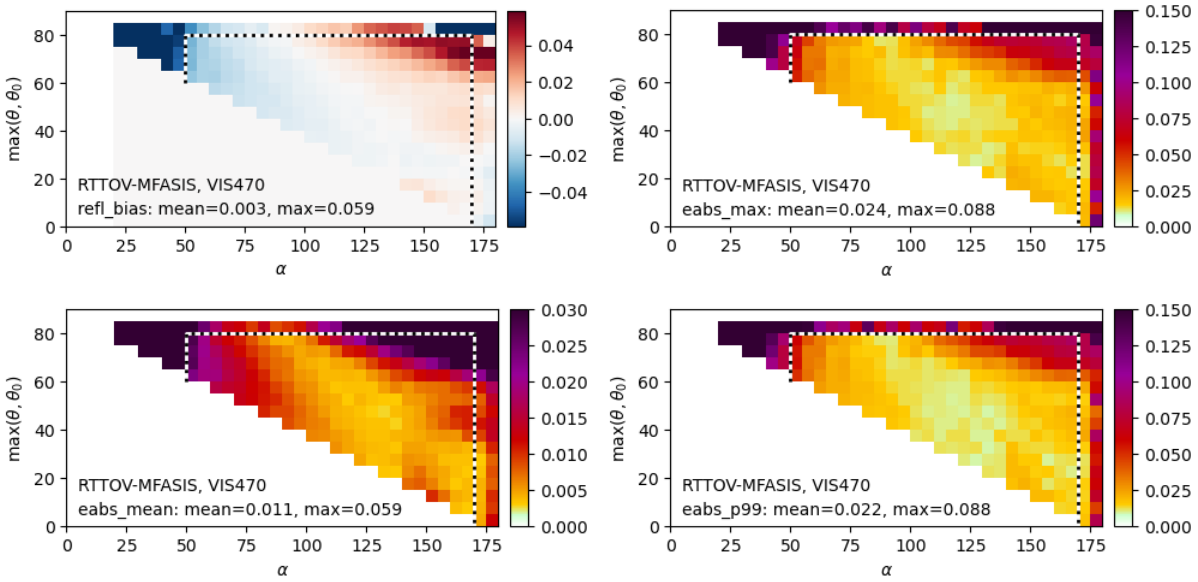

Figure 10: Same as fig. 1 but for the 470nm AMI channel (GEO-KOMPSAT-2A).

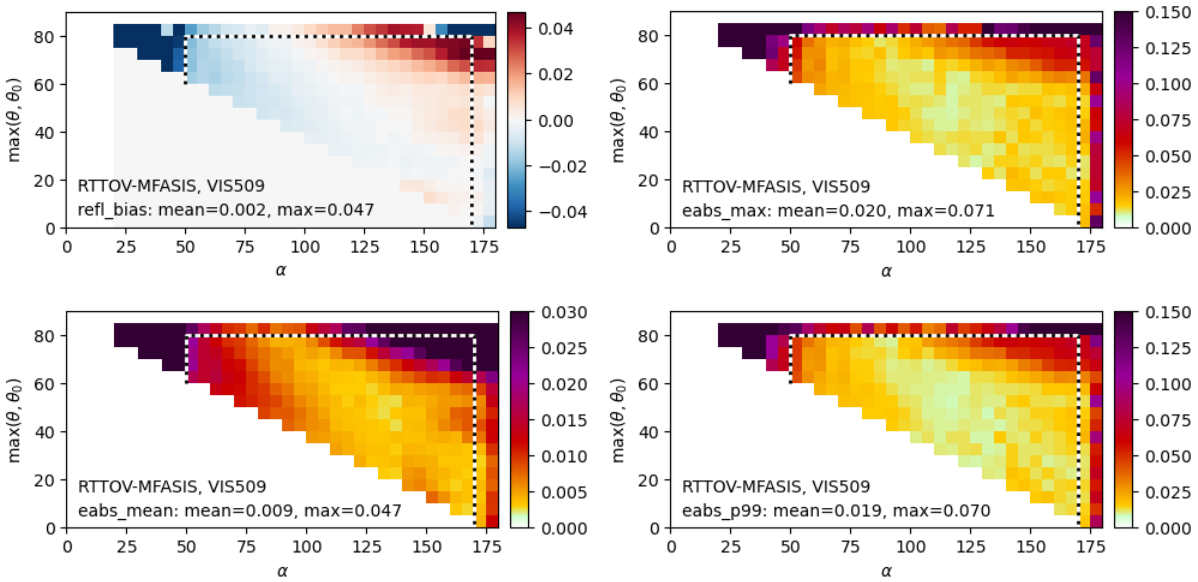

Figure 11: Same as fig. 1 but for the 509nm AMI channel (GEO-KOMPSAT-2A).

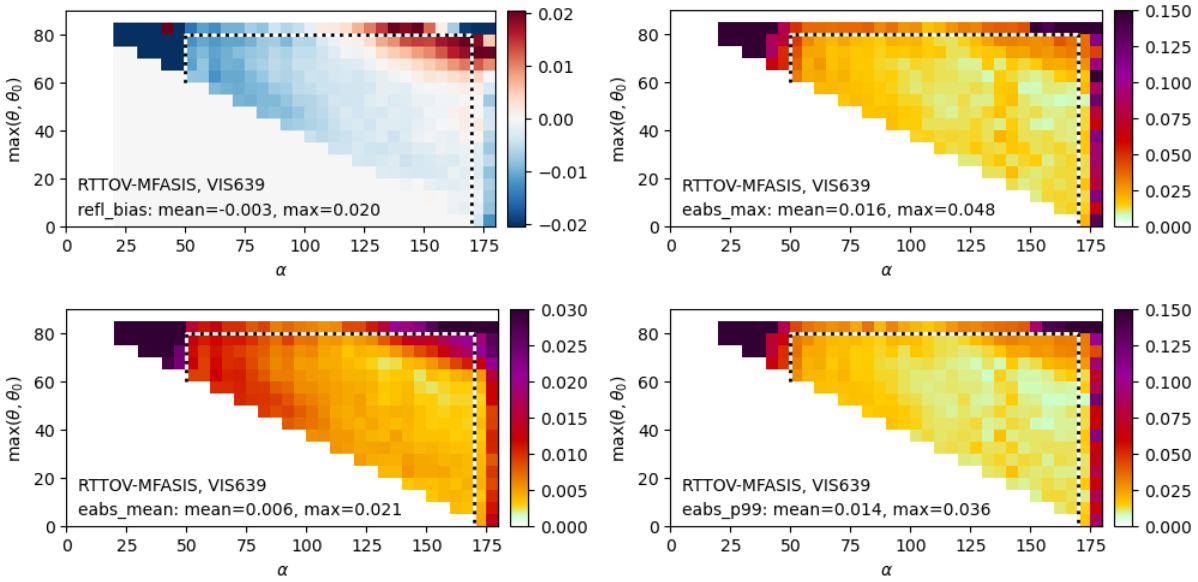

Figure 12: Same as fig. 1 but for the 639nm AMI channel (GEO-KOMPSAT-2A).

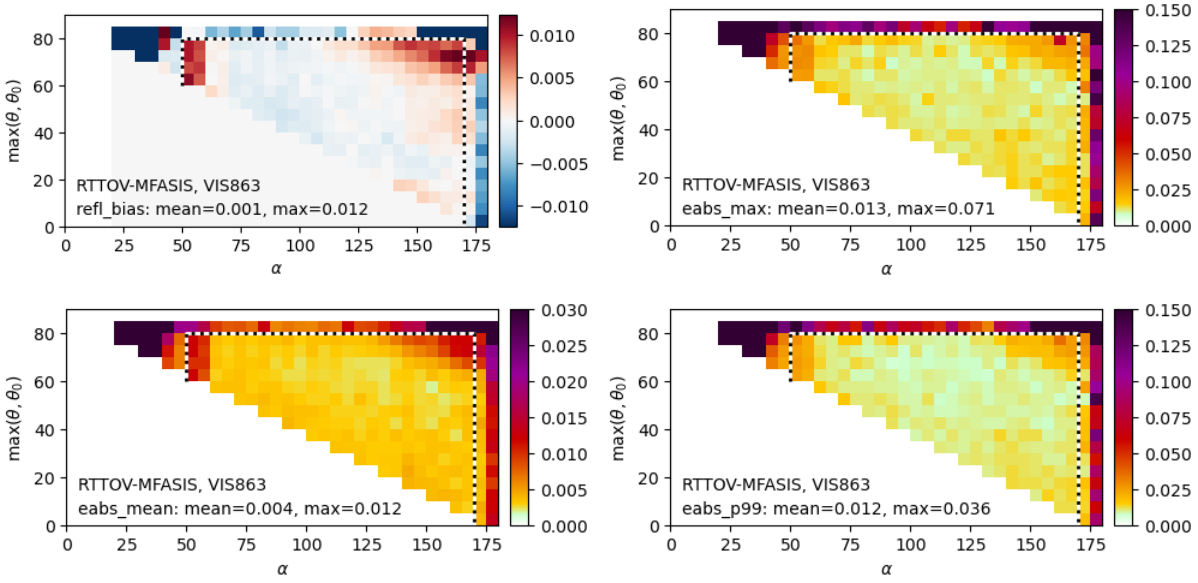

Figure 13: Same as fig. 1 but for the 863nm AMI channel (GEO-KOMPSAT-2A).

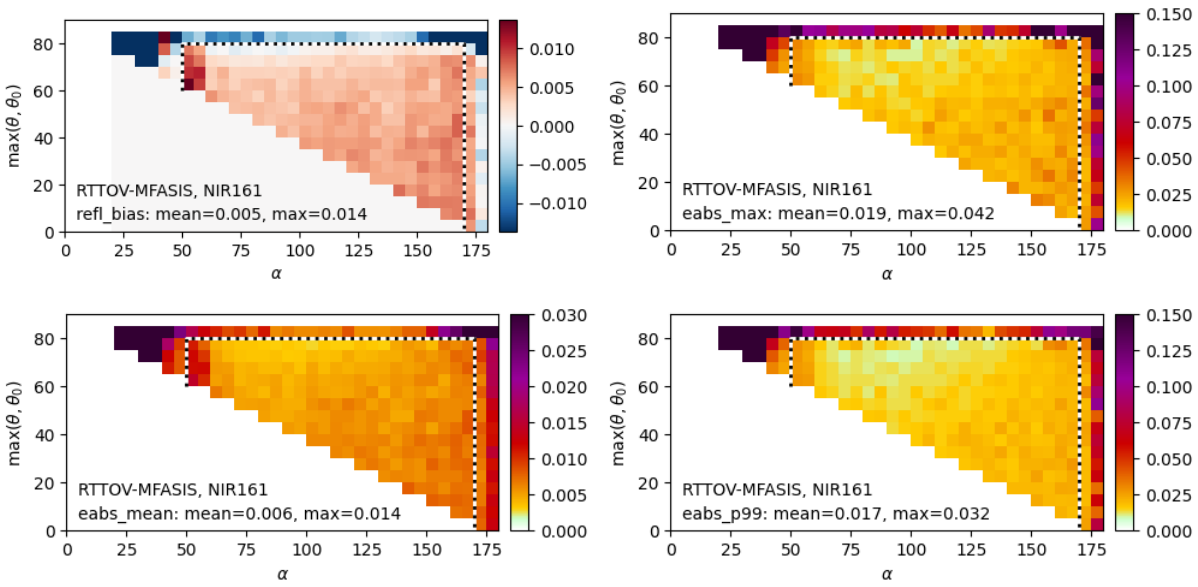

Figure 14: Same as fig. 1 but for the 1610nm AMI channel (GEO-KOMPSAT-2A).

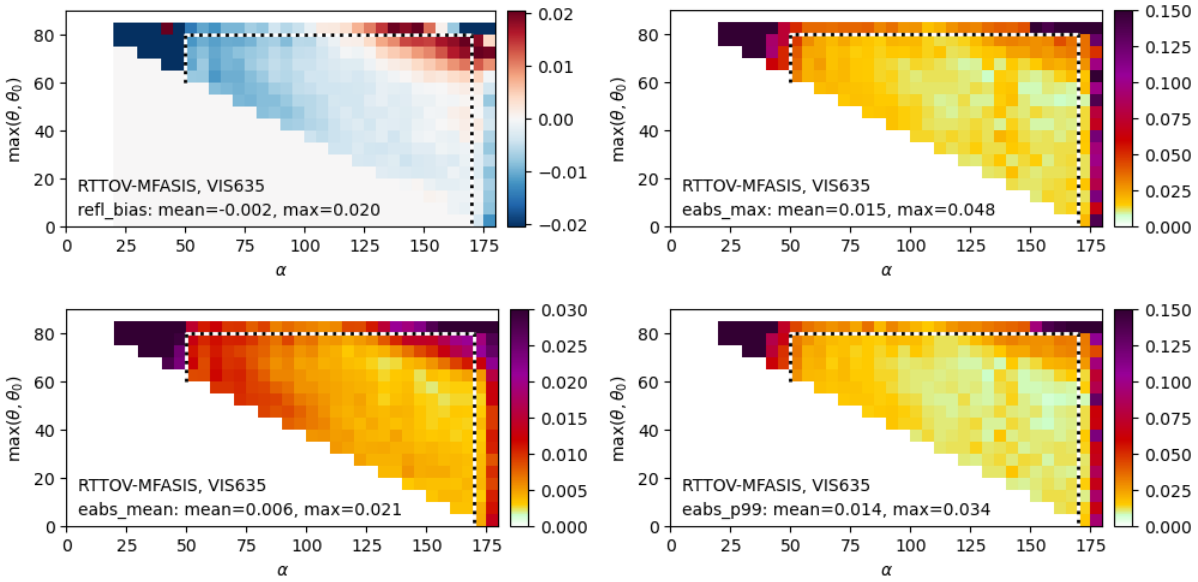

Figure 15: Same as fig. 1 but for the 635nm SEVIRI channel (METEOSAT-11).

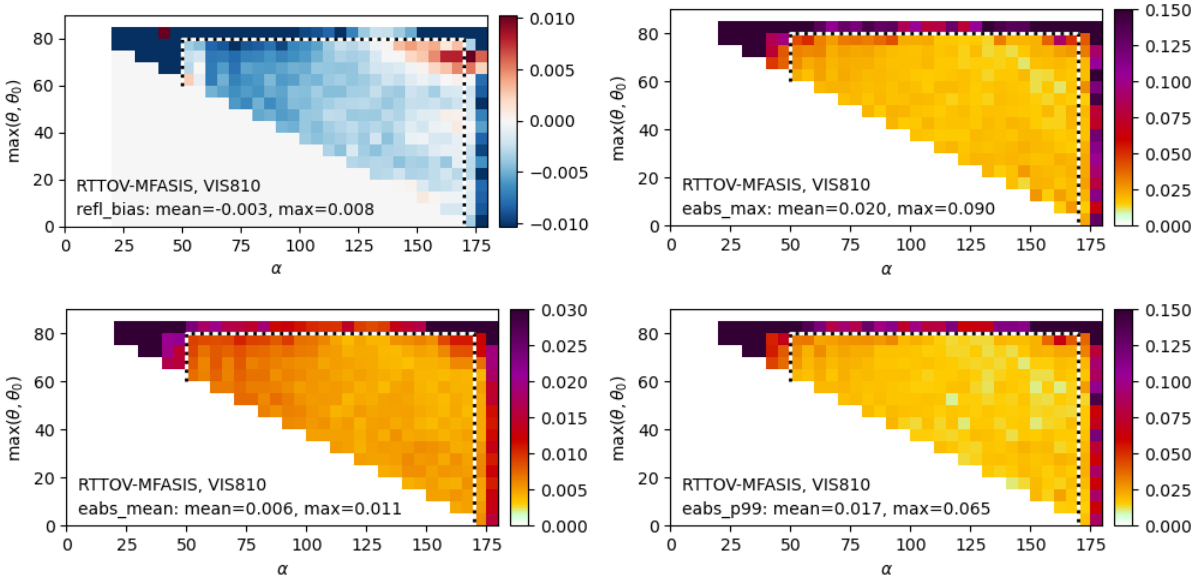

Figure 16: Same as fig. 1 but for the 810nm SEVIRI channel (METEOSAT-11).

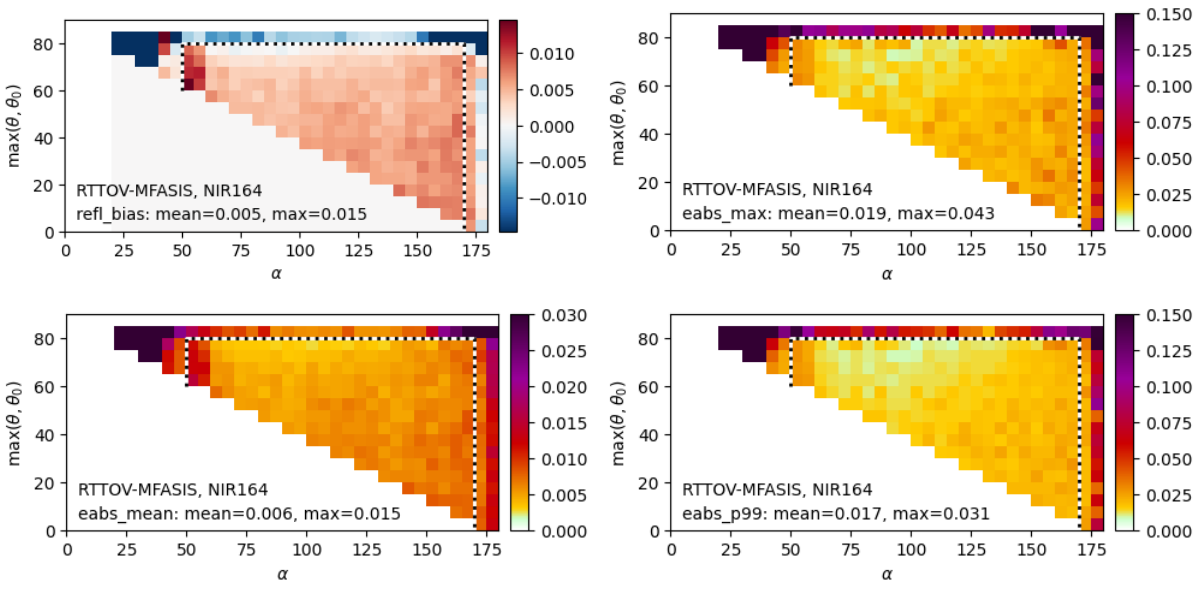

Figure 17: Same as fig. 1 but for the 1640nm SEVIRI channel (METEOSAT-11).

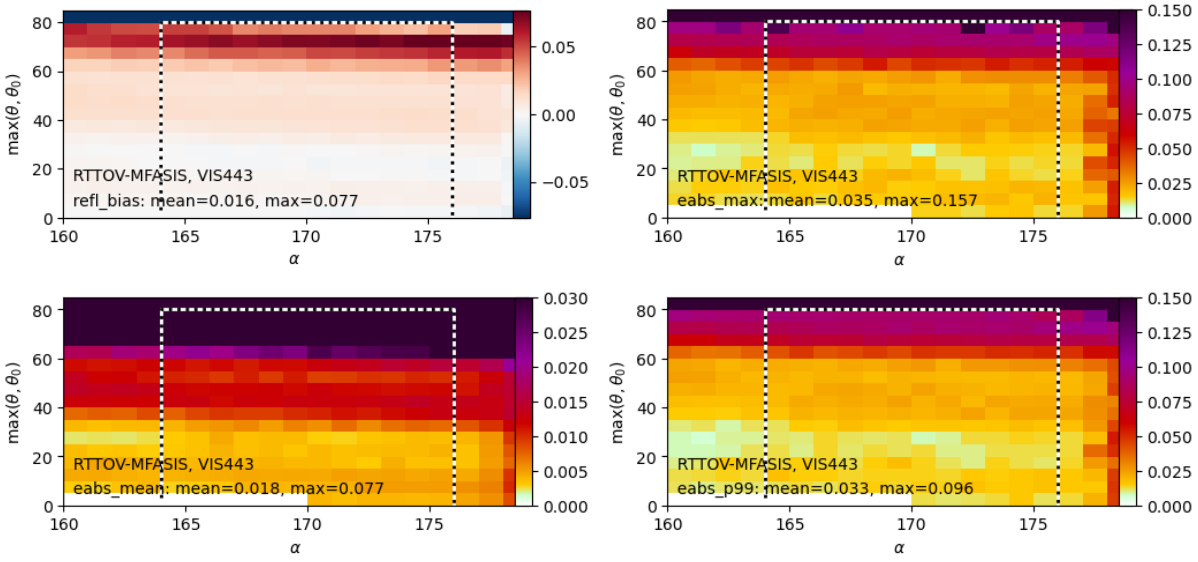

Figure 18: Same as fig. 1 but for the 443nm EPIC channel (DSCOVR-1).

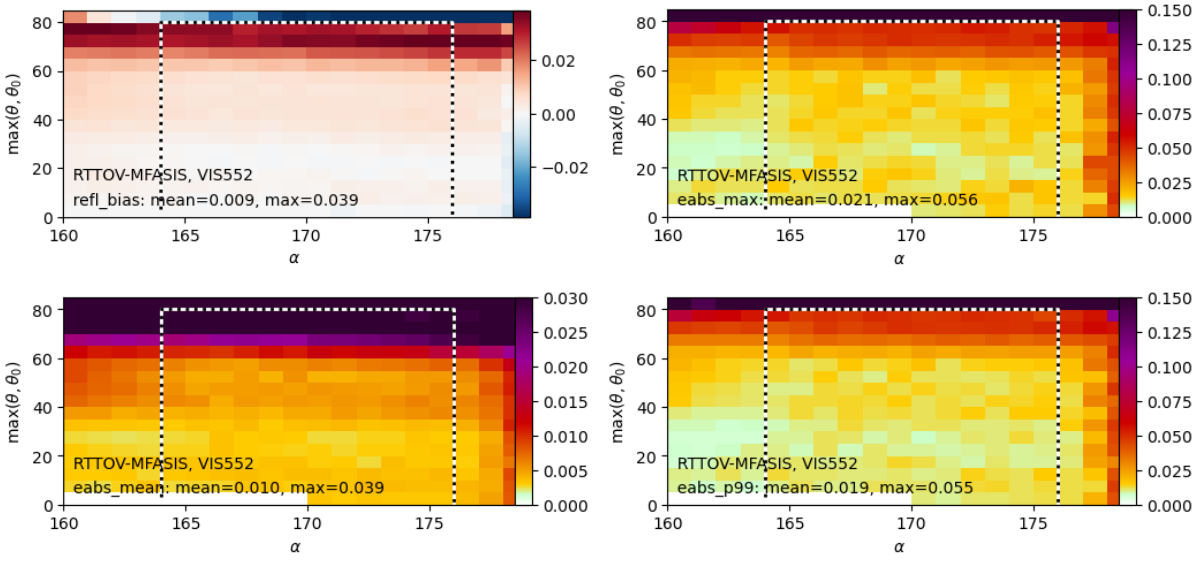

Figure 19: Same as fig. 1 but for the 552nm EPIC channel (DSCOVR-1).

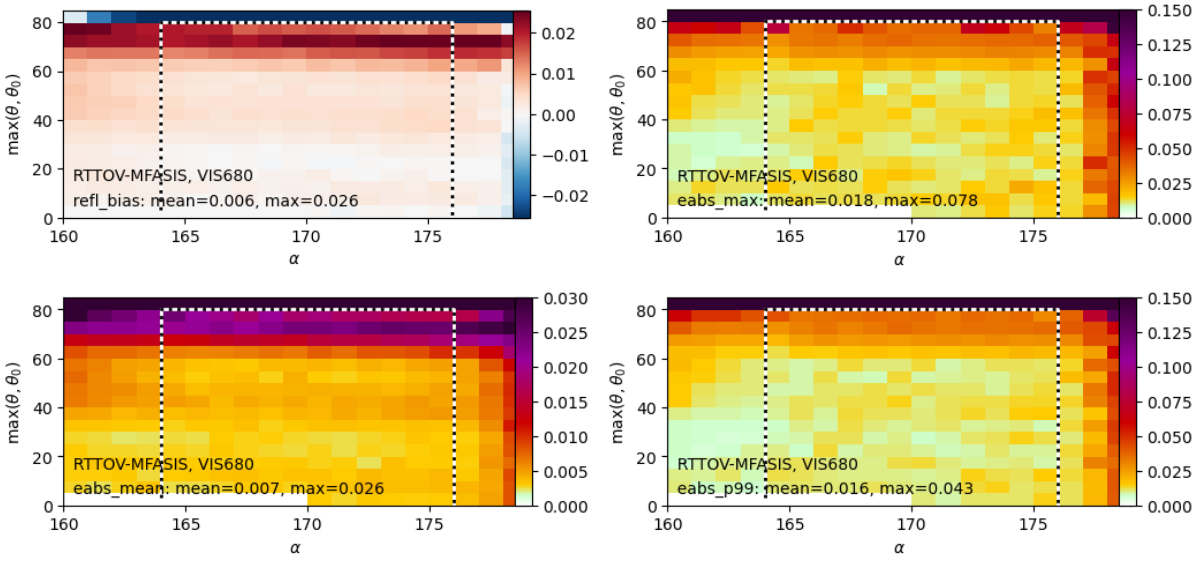

Figure 20: Same as fig. 1 but for the 680nm EPIC channel (DSCOVR-1).

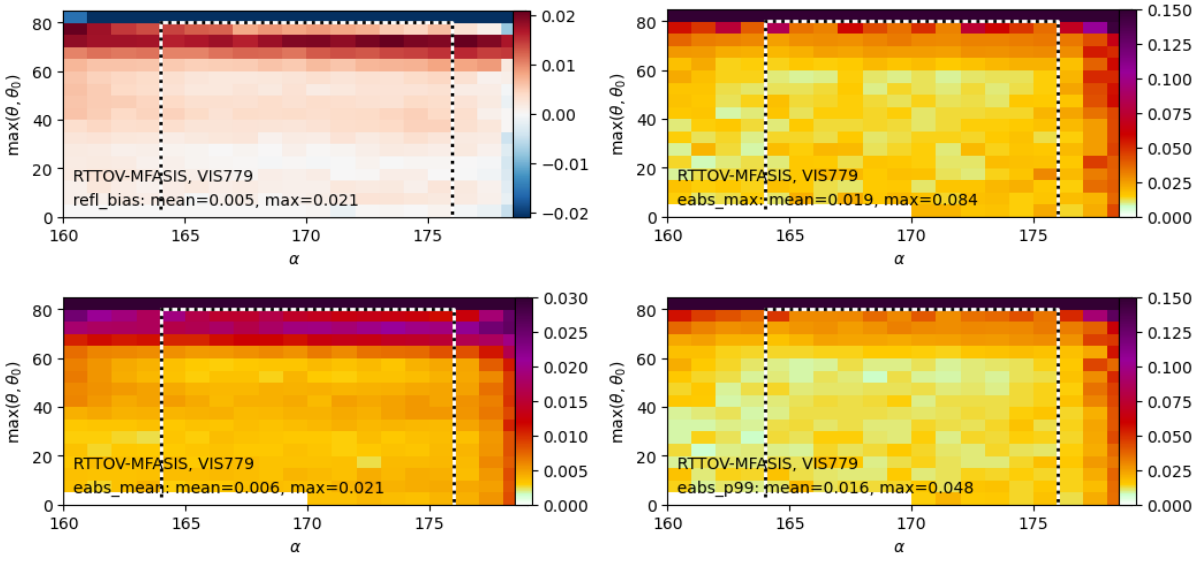

Figure 21: Same as fig. 1 but for the 779nm EPIC channel (DSCOVR-1).

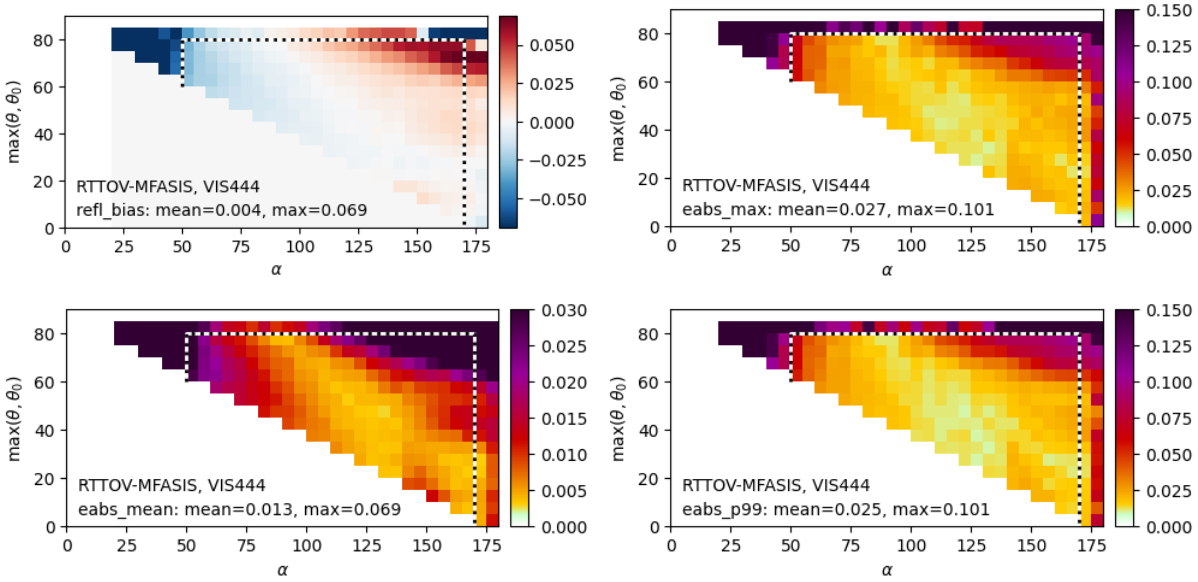

Figure 22: Same as fig. 1 but for the 444nm FCI channel (MTG-I1).

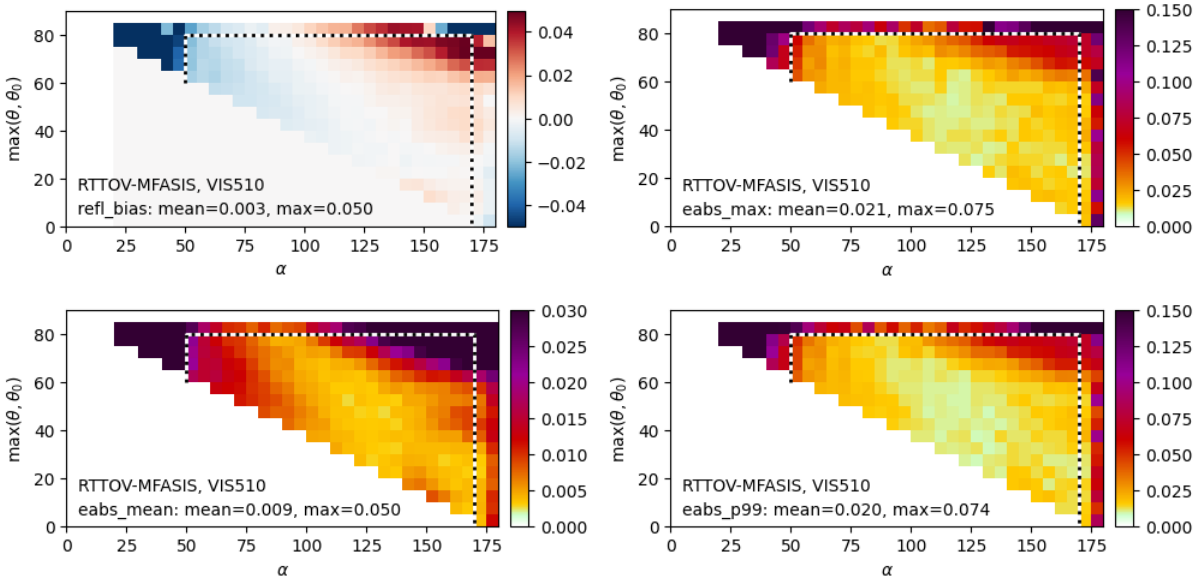

Figure 23: Same as fig. 1 but for the 510nm FCI channel (MTG-I1).

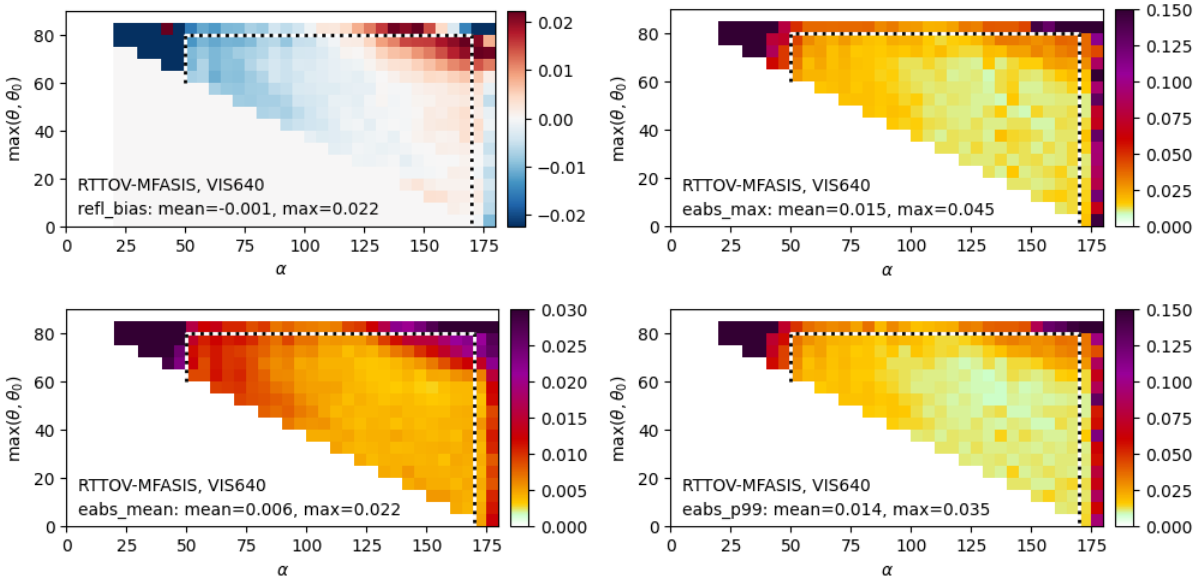

Figure 24: Same as fig. 1 but for the 640nm FCI channel (MTG-I1).

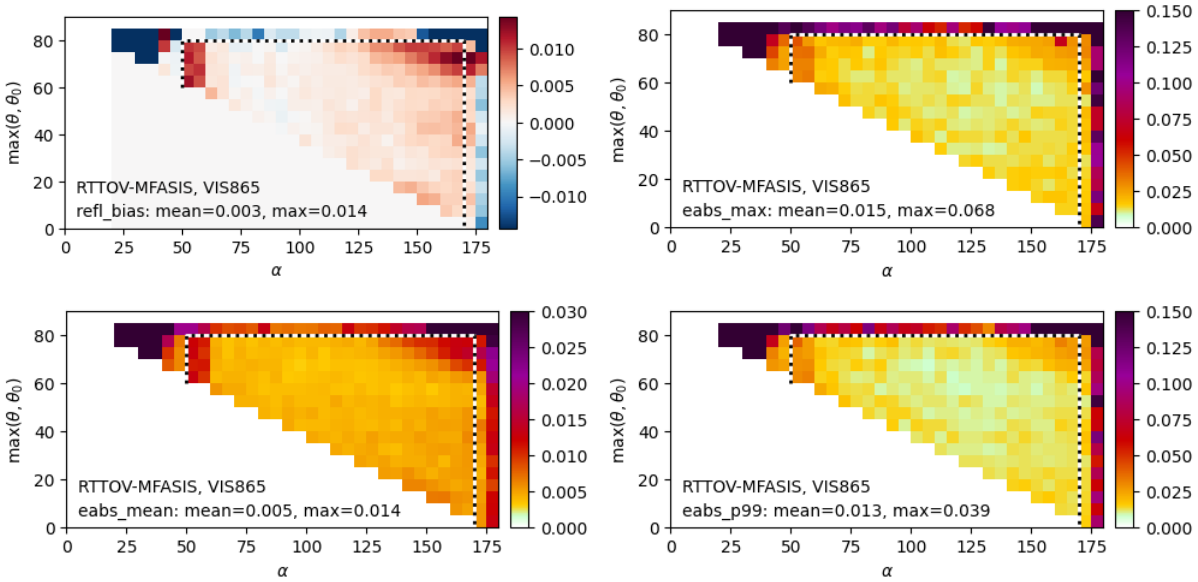

Figure 25: Same as fig. 1 but for the 865nm FCI channel (MTG-I1).

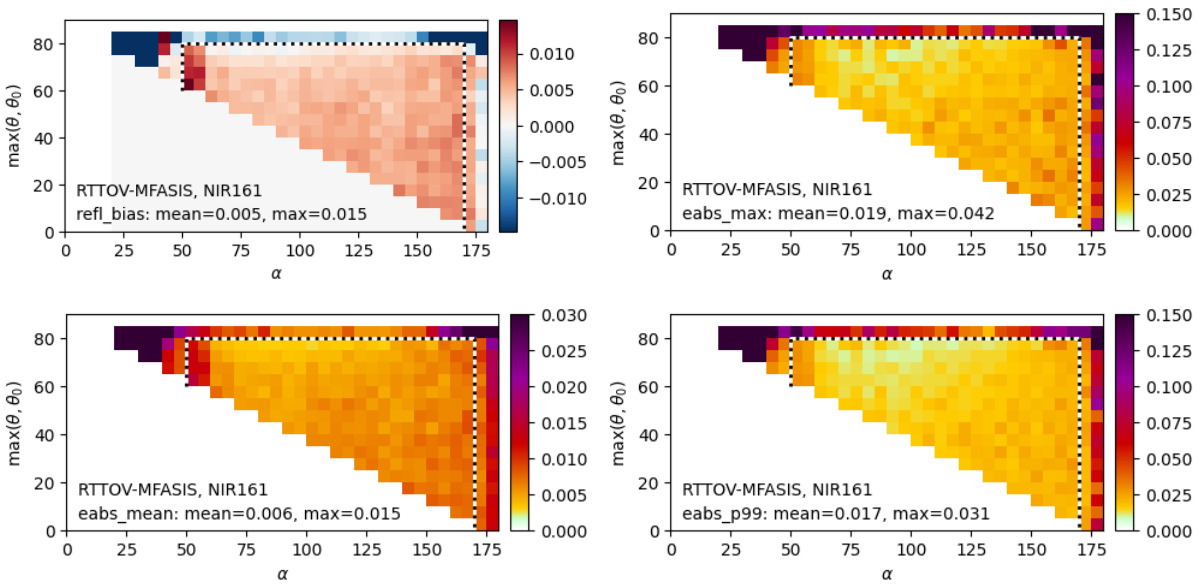

Figure 26: Same as fig. 1 but for the 1610nm FCI channel (MTG-I1).

References

[1] L. Scheck et al. *A fast radiative transfer method for the simulation of visible satellite imagery.* Journal of Quantitative Spectroscopy and Radiative Transfer 175, 54-67, 2016.

[2] R. Saunders et al. *RTTOV-13 Science and Validation Report.* Available at `https://nwp-saf.eumetsat.int/site/download/documentation/rtm/docs_rttov13/rttov13_svr.pdf`.